Published in final edited form as:
Mol Pharm. 2013 June 3; 10(6): 2176–2182. doi:10.1021/mp400087y.

Ex vivo characterization of particle transport in mucus secretions coating freshly excised mucosal tissues

Laura M. Ensign[1,2], **Andreas Henning**[1,2,†], **Craig S. Schneider**[1,2], **Katharina Maisel**[1,3], **Ying-Ying Wang**[1,3], **Marc D. Porosoff**[1,2,‡], **Richard Cone**[1,4], and **Justin Hanes**[1,2,3,5,6,7,*]

[1]Center for Nanomedicine, The Wilmer Eye Institute and Johns Hopkins University School of Medicine, 400 N. Broadway, Baltimore, MD 21231

[2]Department of Chemical and Biomolecular Engineering, Johns Hopkins University, 3400 N. Charles Street, Baltimore, MD 21218

[3]Department of Biomedical Engineering, Johns Hopkins University School of Medicine, 720 Rutland Avenue, Baltimore, MD 21205 (USA)

[4]Department of Biophysics, Johns Hopkins University, 3400 N. Charles Street, Baltimore, MD 21218

[5]Departments of Neurosurgery and Oncology, Johns Hopkins University School of Medicine, 600 N. Wolfe Street, Baltimore, MD 21287 (USA)

[6]Center for Cancer Nanotechnology Excellence, Institute for NanoBioTechnology, Johns Hopkins University, 3400 N Charles Street, Baltimore, MD 21218 (USA)

[7]Department of Ophthalmology, The Wilmer Eye Institute, Johns Hopkins University School of Medicine, 400 N. Broadway, Baltimore, MD 21231

Abstract

Sustained drug delivery to mucosal surfaces has the potential to improve the effectiveness of prophylactic and therapeutic treatments for numerous diseases and conditions, including inflammatory bowel disease, sexually transmitted diseases, cystic fibrosis, glaucoma, dry eye and various cancers. Sustained delivery systems such as nanoparticles can be useful for mucosal delivery, but recent work suggests they should penetrate the rapidly cleared mucus barrier that overlies all mucosal epithelia to achieve uniform distribution on epithelial surfaces and enhanced residence time. Thus, it is important to evaluate mucus-penetrating ability of nano-sized delivery systems in preclinical animal studies, and for administration to humans. We describe a simple *ex vivo* method to visualize and quantify nanoparticle transport in mucus on fresh mucosal tissues. Using this method in murine models, we observed variations in the mucus mesh at various anatomical locations, as well as cyclical variations that may have implications for mucosal delivery.

Keywords

Mucus penetrating particles; particle tracking; drug delivery

[*]To whom correspondence should be addressed: Justin Hanes, Ph.D., 400 N. Broadway, Smith Building 6th floor, Baltimore, MD 21231, Tel: 443-287-7921, Fax: 443-287-7922, hanes@jhmi.edu.
[†]Current Address: Pharmaceutical Development, IDT Biologika, Am Pharmapark 1, Dessau-Rosslau 06861 (Germany)
[‡]Current Address: Department of Chemical Engineering, Center for Catalytic Science and Technology, University of Delaware, 150 Academy Street, Newark, DE 19716

INTRODUCTION

Sustained drug delivery to the mucosal surfaces of the body has potential for improving the treatment and prevention of many diseases, including sexually transmitted infections, inflammatory bowel disease, lung inflammation, and degenerative eye conditions to name only a few. Achieving sustained therapeutic drug concentrations using traditional soluble dosage forms remains challenging due to degradation, rapid shedding, and rapid systemic absorption of drug (3, 4). These difficulties have motivated the development of nano-sized controlled-release carriers for mucosal drug delivery. However, mucosal tissues are protected by mucus layers that not only pose a substantial steric and adhesive barrier to nanoparticles, but are also constantly cleared and renewed (5, 6). To enhance local drug concentrations and residence times, a new approach is to make nanoparticles small enough to penetrate through mucus pores formed by mucin fibers (mesh spacing), that also possess surfaces that do not adhere to mucin fibers (muco-inert surfaces) to avoid adhesive trapping and aggregation of the nanoparticles (7).

Our group pioneered the development of muco-inert mucus penetrating particles (MPP) that diffuse through fresh, undiluted human mucus with speeds only a few-fold lower than their theoretical diffusion in pure water (8, 9). We recently demonstrated that MPP, by penetrating deeper into more slowly cleared mucus layers, provide enhanced distribution and retention in the mouse vagina *in vivo* compared to conventional particles (CP) that are mucoadhesive (1). The ability of MPP to achieve uniform distribution and prolonged retention is likely to lead to significant therapeutic advantages. For example, we have recently shown that acyclovir monophosphate-loaded MPP improved protection against vaginally transmitted HSV-2 compared to 10-fold higher free drug concentration (1). However, development of MPP technology for specific diseases and mucosal surfaces will benefit from a rapid and effective screening method for developing MPP drug carriers. The properties of mucus secretions vary with anatomical location, particularly in disease states where mucus hypersecretion or altered mucin expression is observed (10, 11). Thus, determining whether candidate nanoparticles are mucus-penetrating in a specific mucus secretion is a critical step in proceeding toward efficacy studies.

Fresh, minimally perturbed mucus secretions are in most cases difficult to obtain, and mucus secretions are often obtained by mechanical removal (lavaging, scraping, swabbing, suction, etc.) from the epithelial surface (12, 13). Much of our previous work was facilitated by using a self-sampling menstrual collection device (13) that provides fresh, minimally-perturbed human cervicovaginal mucus (hCVM). However, for less accessible mucosal surfaces, such as those of the colon or airways, non-invasive collection of sufficient quantities of undiluted mucus is quite difficult. Here, we describe a method for characterizing particle transport in mucus secretions directly on the surface of *ex vivo* tissue samples, and validate this technique using mouse gastrointestinal, reproductive, and respiratory tissues.

EXPERIMENTAL SECTION

All experiments were conducted with female 6–8 week old CF-1 mice (Harlan) following protocols approved by the Johns Hopkins University Animal Care and Use Committee.

Particle formulation and multiple particle tracking

MPP of various sizes were made by covalently coating the surfaces of fluorescent carboxyl-modified polystyrene nanoparticles (Molecular Probes) with a high density of low molecular weight (2 or 5 kDa) polyethylene glycol (Creative PEGworks) via standard 1-ethyl-3-(3-dimethylaminopropyl) carbodiimide coupling reaction (14). CP were uncoated carboxyl-

modified polystyrene nanoparticles. Particles were suspended in hypotonic solution (ultrapure water) for administration. Particle size and ξ-potential were determined by dynamic light scattering and laser Doppler anemometry, respectively, using a Zetasizer Nano ZS90 (Malvern Instruments). Size measurements were performed at 25°C at a scattering angle of 90°. Samples were diluted in 10 mM NaCl solution (pH 7) and measurements performed according to instrument instructions. As previously (15), successful PEG coating was reflected by neutralization of the surface charge, resulting in a ζ-potential more neutral than −10 mV (Table 1). PEG on the MPP surface was in the "brush" conformation, providing a dense coating that effectively shields the particle from adhesion to hCVM and brain tissue (14). MPP and CP were tested in healthy human cervicovaginal mucus (hCVM) to confirm mucus-penetrating ability and mucoadhesion, respectively, prior to testing in *ex vivo* tissue samples (data not shown). Particle motions were recorded using an Evolve 512 EMCCD camera (Photometrics) mounted on an inverted epi-fluorescence microscope (Axio Obxerver D1, Zeiss) with a 100X/1.4 NA objective and the appropriate filters. Movies were captured with Metamorph software (Molecular Devices) at a temporal resolution of 66.7 ms for 20 s. The coordinates of nanoparticle centroids were transformed into time-averaged mean-square displacements (MSD) calculated as $\langle \Delta r^2(\tau) \rangle = [x(t+\tau) - x(t)]^2 + [y(t+\tau) - y(t)]^2$, where x and y represent the nanoparticle coordinates at a given time and t is the time scale (8, 9). Mucus samples were assumed to be locally isotropic (but not necessarily homogeneous), such that 2D diffusion can be extrapolated to 3D diffusion as described (16). We have previously estimated that the static error for our system is on the order of 20 nm, which is much smaller than the overall particle displacements (17). Although we are unable to determine the dynamic error for MPP in a complex, viscoelastic fluid such as mucus, we compare data at a time scale (1 s) that is long relative to the time interval between frames to minimize contributions of dynamic error.

Ex vivo tracking

Gastrointestinal tract—Mice were fed a liquid diet for three days and then starved overnight to reduce the amount of solid content in the gastrointestinal tract, before being sacrificed for tissue collection. The colon or small intestine was gently removed and carefully sliced open longitudinally. To collect mucus, the smooth surface of a 10 μL capillary pipette (Wiretrol®, Drummond Scientific) was used to gently scrape along the luminal tissue surface, and the mucus was used for particle tracking studies (described below) in a custom-made 5 μL well. Alternatively, a small section of tissue approximately 0.5 cm x 1 cm was placed in a custom rectangular well. To ensure adequate particle distribution and concentration for imaging, a small volume (0.25 μL) of dilute particle solution (0.02–0.08% w/v) was carefully pipetted directly onto the surface of the mucus, utilizing capillary flow to merely contact the mucus surface with the droplet suspended from the end of the pipet tip. This was repeated in at least 5 areas of contact to ensure that there was no pooling of fluid and that the particles were well distributed over the entire surface (fluorescent coverage of the entire mucosal surface was visually confirmed at low magnification). The depth of the well was adjusted such that a cover slip used to seal the well would contact the mucus surface without compressing the tissue. Superglue was used to quickly seal the prepared sample and minimize dehydration prior to imaging. Tissue topography was evident when imaging the colon tissues; some dark areas of tissue, likely villi projecting from the tissue surface, were apparent with particles diffusing in the mucus in between. We did not observe tissue topography when imaging the small intestine tissue, which was likely due to the very thick mucus layer observed on top of the tissues.

Female reproductive tract—Mice were either given a subcutaneous injection of 2.5 mg of Depo Provera® (UpJohn) to induce a diestrus-like state (DP) commonly used in mouse models of vaginal delivery, or mice were selected during the estrus phase (1). Since the

vagina has relatively less surface area than the GI or respiratory tract tissues, particles could be directly administered to the vagina with adequate concentration and distribution for imaging. No qualitative difference in particle transport was observed whether the particles were administered in the vagina or onto the excised tissue surface (not shown). Particles (5 μL) were administered vaginally prior to sacrifice and tissue removal to allow for osmotically-driven absorption of excess fluid (1). The entire vaginal tract (cut below the cervix) was excised and sliced open longitudinally. The tissue was placed luminal side up in a custom rectangular well. The depth of the well was adjusted for the characteristic tissue thickness in each hormonal state such that a cover slip used to seal the well would contact the mucus surface without compressing the tissue. Superglue was used to quickly seal the prepared sample and minimize dehydration prior to imaging. Tissue topography was not apparent when imaging vaginal tissue.

Respiratory tract—A small piece of mouse trachea (~ 5mm) was dissected. The trachea was cut open longitudinally and placed mucosal side up on a glass slide. To ensure adequate particle distribution and concentration for imaging, a low volume (0.1 μL) of particles was applied directly to the luminal surface of the section, and the trachea was promptly sealed with a coverslip using a thin layer of super glue around the periphery of the coverslip to minimize dehydration prior to imaging. Tissue topography was not apparent when imaging trachea tissue, and particles were only imaged in areas without active cilia beating.

Nanoparticle distribution in the female reproductive tract

Five μL of either CPs or MPPs were administered intravaginally to either estrus phase mice or DP mice. After 10 min, the entire vagina was then removed and frozen in Tissue-Tek O.C.T. Compound (Sakura Finetek U.S.A., Inc.). Transverse sections were obtained at various points along the length of the tissue using a Microm HM 500 M Cryostat (Microm International). The thickness of the sections was set to 6 μm to achieve single cell layer thickness. The sections were then stained with ProLong Gold (Invitrogen) antifade reagent with DAPI to visualize cell nuclei and retain particle fluorescence. Fluorescent images of the sections were obtained with an inverted fluorescent microscope.

Statistical analysis

All data are presented as a mean with standard error of the mean (SEM) indicated. Statistical significance was determined by a two-tailed, Student's t-test ($\alpha = 0.05$) assuming unequal variance.

RESULTS

Tracking on *ex vivo* colon tissue versus isolated colon mucus

We first sought to determine whether nanoparticle transport behavior is similar in colonic mucus on the surface of freshly excised (*ex vivo)* mouse colon tissue as compared to mucus that was gently scraped from the tissue surface. As shown in Fig. 1A, the trajectories of representative 100 nm MPP particles (polystyrene particles with a dense coating of PEG) both in collected mucus and on *ex vivo* colon tissue were indicative of diffusion, whereas 100 nm CP particle (carboxyl-modified polystyrene particles) motions were highly restricted due to mucoadhesion. The ensemble-averaged mean-squared displacements (<MSD>) of MPP particles were not statistically different between collected colonic mucus and *ex vivo* colon tissue at any time scale up to 3 sec (similar for CP), suggesting that the handling of the *ex vivo* tissue did not perturb the mucus layer (Fig. 1B). However, MPP were significantly slowed in mouse colonic mucus compared to the same particles in human cervicovaginal mucus (hCVM), implying that the average pore size of mouse colonic mucus is likely smaller than the reported value for hCVM, 340 ± 70 nm (7). To further investigate this

possibility, we tested 40 nm and 200 nm MPP and CP on *ex vivo* colon tissue. As expected, the <MSD> for 40 nm MPP was about 2-fold higher than for 100 nm MPP. However, 200nm MPP were constrained, resulting in <MSD> values similar to all sizes (40–200 nm) of CP (Fig. 2A). Since MPP would not be adhesively trapped in mucus, it is likely that the average mesh spacing in mouse colon mucus is small enough to physically trap nanoparticles 200 nm in diameter. Indeed, the effective diffusivity (D_{eff}) values calculated for 200 nm MPPs and CPs were likely indicative of motion due to thermal fluctuation of the mucus gel, not diffusion (Fig. 2B, dashed lines). As shown in Figure 2C, even the fastest 10% of 100 nm MPP were ~24-fold slower than their theoretical diffusion in water, indicating that there was significant physical restriction to diffusion for a particle this size.

Tracking on *ex vivo* small intestine tissue

We then probed the mucus mesh of mouse small intestine (SI) mucus using freshly excised (*ex vivo)* tissue samples. As shown in Figure 3A, the <MSD> for 200 nm MPP was about two-fold lower than for 100 nm MPP at a time-scale of 1 sec, as would be expected. However, 500 nm MPP were completely immobilized, such that the <MSD> was indistinguishable from <MSD> measured for CP of various sizes. The steric trapping of 500 nm MPP indicates that the range of pore sizes in mouse small intestine mucus is narrower than the reported range for hCVM, because 500 nm MPP diffuse in hCVM (2, 8). Additionally, many of the 200 nm MPP had D_{eff} values corresponding to an <MSD> less than the particle diameter, likely indicating trapped particles exhibiting thermal fluctuations of the mucins (Fig. 3B). As shown in Figure 3C, the top 10% of 200 nm MPP were only ~3-fold slower than their theoretical diffusion in water, whereas particles below the 50^{th} percentile were slowed 20-fold or greater. It is evident that mouse small intestine mucus is permeable to larger nanoparticles than mouse colon mucus.

Tracking on *ex vivo* vaginal tissue

While it is likely that the characteristics of mucus change with different disease states, it is also possible that there is cyclical variation in the female reproductive tract of healthy women. For instance, it is known that the properties of cervicovaginal mucus can vary throughout the menstrual cycle (18). Consequently, the estrous cycle of a mouse may have an effect on the properties of mouse cervicovaginal mucus. One common way to synchronize the estrous cycle of mice for vaginal studies is to administer a subcutaneous injection of Depo Provera, a synthetic progestin. Depo Provera treatment effectively arrests the estrous cycle in a state similar to the diestrus phase and is associated with a thickening of the vaginal mucus (19). In contrast, the estrus phase of the estrous cycle is dominated by estrogen, which induces secretion of more watery mucus (20). As shown in Fig 4A, the <MSD> of 100 nm MPP on *ex vivo* estrus vaginal tissue was very similar to that in hCVM. However, the <MSD> of 100 nm MPP on *ex vivo* DP vaginal tissue at a time of 1 sec was >30-fold lower than estrus phase vaginal tissue. To further investigate the difference in transport rates, we examined the distribution of particle effective diffusivities (Fig 4B). On estrus vaginal tissue, 70% of MPP were faster than all MPP on DP vaginal tissue. Also, 23% of MPP on DP vaginal tissue had diffusivity values corresponding to an MSD less than the particle diameter, suggesting that these particles were moving only as a result of thermal fluctuations of the mucus gel; these particles were likely trapped by the mucus mesh due to steric interactions.

Recently, we demonstrated that MPP capable of rapid diffusion on estrus vaginal tissue were able to rapidly and evenly distribute in the mouse vagina when administered in hypotonic medium, causing the particles to be drawn osmotically through the mucus to the surface of the vaginal epithelium (1). Thus we compared the distribution of MPP administered hypotonically in the estrus and DP mouse vagina. In Figure 4C, it is evident that MPP able

to penetrate estrus vaginal mucus in *ex vivo* preparations are also able to distribute evenly over the vaginal tissue surface, including the deep folds (rugae). In contrast, MPP that are more hindered in DP vaginal mucus in *ex vivo* preparations are drawn non-uniformly to the vaginal epithelium of mice treated with DP, and many particles remain in the luminal mucus layer (Fig 4D).

Tracking on *ex vivo* tracheal tissue, comparison to all mucosal tissues

The airways are also of particular interest for mucosal drug delivery. Mucus turnover is especially rapid in the airways, perhaps due to persistent exposure to inhaled foreign particulate matter. Ciliated epithelial cells transport airway mucus against gravity out of the airways such that any trapped material will be swallowed and digested. Drug delivery vehicles that are muco-inert may be cleared more slowly, thereby allowing improved drug delivery (6). Similar to all other tissues tested, 100 nm MPP were generally diffusive, whereas 100 nm CP were immobilized, in fresh tracheal tissue mucus layers. Comparing the <MSD> of 100 nm MPP on trachea tissue to the same particles in hCVM and on all other *ex vivo* tissues tested (Figure 5A), it was evident that there was a wide range of transport rates. The average effective diffusion coefficient (D_{eff}) at a time scale of 1 s was calculated for 100 nm MPP in each mucus type (Figure 5B). In estrus vaginal mucus, 100 nm MPP are only slowed 8-fold compared to water in (1), indicating the mucus mesh is similar to that of hCVM. In contrast, 100 nm MPP are slowed >260-fold in DP vaginal mucus compared to in water. The D_{eff} values for 100 nm MPP in mucus covering the epithelium of the small intestine, trachea, and colon mucus were slowed ~30-, 80-, and 90-fold, respectively, compared to their theoretical diffusion in water.

DISCUSSION

The mucus layers that protect epithelial surfaces have been highlighted as a significant barrier to nanoscale drug and gene delivery vehicles (5, 6, 21). Although mucus serves to protect and lubricate all mucosal epithelia, its properties can vary at different anatomical locations and in disease states. To assess the transport properties of nano-sized drug and gene delivery vehicles, it is important to obtain unadulterated mucus samples to ensure that the vital structural properties of mucus are maintained. Here, we demonstrate that nanoparticle transport in mucus can be characterized directly on mucosal tissue freshly obtained from animals, and that the same muco-inert MPP diffused at different rates on mucosal tissue obtained from various anatomical locations in the mouse. It is possible that the unique rheological and barrier properties required at each mucosal surface give rise to different mesh spacings or other structural properties, which has important implications for mucosal drug and gene delivery.

We found that larger MPP can penetrate mouse small intestine mucus than mouse colon mucus, which may be a reflection of the different functions of the mucosa. The small intestine is the primary site for nutrient absorption, whereas the colonic mucosa must be a barrier to the dense bacterial population colonizing the mucosa (22, 23). Also, we found that polystyrene particles are mucoadhesive, consistent with the known hydrophobic barrier properties of gastrointestinal mucus (23). In contrast to our results on *ex vivo* particle diffusion, another study in samples of pig small intestine mucus found that 500 nm polystyrene particles were immobilized, but polystyrene particles as large as 2 μm were able to diffuse when coated with bile salts. The fact that much larger particles diffused through pig, but not mouse, small intestine mucus could be due to a difference between species, or it could result from the washing and freezing involved in the pig small intestine mucus collection (24). Similarly, other studies found that uncoated polystyrene nanoparticles diffuse in pig intestinal mucus, but again these studies did not use *ex vivo* mucosal tissue,

relying instead on reconstituted mucin solutions or frozen samples obtained hours after slaughter (12, 25).

Variation in vaginal mucus properties is particularly important for rodent studies involving vaginal delivery, because significant changes to the vaginal mucosa happen throughout the estrous cycle over a 4–5 day period (26). For example, mice are known to be far more susceptible to *N. gonorrhoeae* infection in the proestrus or estrus phase (27), and more susceptible to HSV-2 infection when in a diestrus-like phase induced by Depo Provera treatment (28). We demonstrate here that the estrus phase vaginal mucus is comparatively more penetrable by 100 nm MPP than DP vaginal mucus. The mouse vaginal epithelium in the estrus phase most closely resembles that of the human vagina (29, 30), and MPP penetrate estrus phase mouse vaginal mucus at rates comparable to MPP penetration in hCVM (1). The relatively smaller mesh of DP mouse vaginal mucus may be important, considering that this mouse model is commonly used for vaginal drug delivery (31–33). Previous studies of vaginal drug and nucleic acid delivery have employed the use of vaginal lavages, swabs, or degradative enzymes to diminish the mucus barrier properties (33–36). We found that removing vaginal mucus led to improved distribution of mucoadhesive nanoparticles throughout the vaginal tract (1). Similarly, it was previously demonstrated on *ex vivo* tracheal tissue that gene carriers more rapidly penetrated mouse tracheal mucus after mucolytic treatment, leading to improved transfection in the airways *in vivo* with mucolytic treatment (11). We demonstrated here that the relatively hindered transport of MPP *ex vivo* in DP mouse vaginal mucus, as compared to MPP in estrus phase vaginal mucus, resulted in superior MPP distribution in the estrus phase mouse vagina. It has been recently suggested that particle diffusion over relatively short distances, as is the case of the particle tracking data shown here, cannot be extrapolated to describe transport through physiologically relevant mucus thicknesses, at least in the airways (37). We have observed a correlation between rapid diffusion of MPP over a short distance (~1 μm^2) in *ex vivo* hCVM and the ability of that same MPP to diffuse rapidly in *ex vivo* mouse CVM and, when delivered hypotonically, to traverse the mucus layer *in vivo* to reach the vaginal epithelium in less than 10 min (Fig 4C) (1). Whether or not the same will occur in the airways is yet to be determined. In addition, we demonstrate here that hindered diffusion of nanoparticles in *ex vivo* mouse vaginal mucus correlates to hindered transport of these nanoparticles to the vaginal epithelium when delivered hypotonically *in vivo* (Fig 4D).

It is important to note that the density of PEG on the nanoparticle surface greatly impacts the adhesiveness of the particles. Here we use MPP with a PEG surface density that is sufficient for penetration through various human mucus secretions as well as human and rodent brain tissue (14), though it is impossible to completely rule out potential interaction between mouse mucus and the MPP used for this work. Accordingly, the apparent pore structure inferred by the diameter of nanoparticles used includes both steric and potential adhesive interaction effects. The mesh spacing of human mucus at most mucosal surfaces is still unknown, thought we have previously demonstrated that MPP as large as 500 nm could penetrate hCVM (7), and MPP as large as 200 nm could penetrate through sputum expectorated from cystic fibrosis patients (38), tracheal mucus obtained from patients without lung disease (39), and human chronic rhinosinusitis mucus (40). Variations in mesh spacing have important implications for the understanding both the transmission of infections at mucosal epithelia and for mucosal drug delivery using nanotechnology. It is possible to obtain vaginal (41) and colonic tissue (42) samples from human patients, which could then be tested with the methods reported here to ensure that nanoparticles engineered to treat mucosal surfaces will penetrate the mucus at the intended location of delivery. It is also true that this simple, but useful technique can be implemented to ensure that mucosal drug delivery systems tested in animal models can be modified as needed for human patients prior to costly and time consuming clinical trials.

Acknowledgments

We thank Tim Hoen for his training and assistance with animal handling and the Wilmer Microscopy and Imaging Core Facility (grant EY001765). This work was supported by the NIH (grants R33AI079740, R01CA140746, R21AI094519, U54CA151838), the Cystic Fibrosis Foundation (grant HANES07XX0), and National Science Foundation (L.M.E., K.M.,Y-Y.W.) and Howard Hughes Medical Institute (L.M.E, C.S.) graduate research fellowships. The mucus penetrating particle technology described in this publication is being developed by Kala Pharmaceuticals. Dr. Hanes is co-founder and consultant of Kala. Drs. Hanes and Cone own company stock, which is subject to certain restrictions under University policy.

References

1. Ensign LM, et al. Mucus-penetrating nanoparticles for vaginal drug delivery protect against herpes simplex virus. Sci Transl Med. 2012; 4(138):138ra179.
2. Lai SK, Wang YY, Cone R, Wirtz D, Hanes J. Altering mucus rheology to “solidify” human mucus at the nanoscale. PLoS One. 2009; 4(1):e4294. [PubMed: 19173002]
3. des Rieux A, Fievez V, Garinot M, Schneider YJ, Preat V. Nanoparticles as potential oral delivery systems of proteins and vaccines: a mechanistic approach. J Control Release. 2006; 116(1):1–27. [PubMed: 17050027]
4. Mallipeddi R, Rohan LC. Nanoparticle-based vaginal drug delivery systems for HIV prevention. Expert Opin Drug Deliv. 2010; 7(1):37–48. [PubMed: 20017659]
5. Cone RA. Barrier properties of mucus. Adv Drug Deliv Rev. 2009; 61(2):75–85. [PubMed: 19135107]
6. Lai SK, Wang YY, Hanes J. Mucus-penetrating nanoparticles for drug and gene delivery to mucosal tissues. Adv Drug Deliv Rev. 2009; 61(2):158–171. [PubMed: 19133304]
7. Lai SK, Wang YY, Hida K, Cone R, Hanes J. Nanoparticles reveal that human cervicovaginal mucus is riddled with pores larger than viruses. Proc Natl Acad Sci U S A. 2010; 107(2):598–603. [PubMed: 20018745]
8. Lai SK, et al. Rapid transport of large polymeric nanoparticles in fresh undiluted human mucus. Proc Natl Acad Sci U S A. 2007; 104(5):1482–1487. [PubMed: 17244708]
9. Dawson M, Wirtz D, Hanes J. Enhanced viscoelasticity of human cystic fibrotic sputum correlates with increasing microheterogeneity in particle transport. J Biol Chem. 2003; 278(50):50393–50401. [PubMed: 13679362]
10. Kararli TT. Comparison of the gastrointestinal anatomy, physiology, and biochemistry of humans and commonly used laboratory animals. Biopharm Drug Dispos. 1995; 16(5):351–380. [PubMed: 8527686]
11. Suk JS, et al. N-acetylcysteine enhances cystic fibrosis sputum penetration and airway gene transfer by highly compacted DNA nanoparticles. Mol Ther. 2011; 19(11):1981–1989. [PubMed: 21829177]
12. Crater JS, Carrier RL. Barrier properties of gastrointestinal mucus to nanoparticle transport. Macromol Biosci. 2010; 10(12):1473–1483. [PubMed: 20857389]
13. Olmsted SS, et al. Diffusion of macromolecules and virus-like particles in human cervical mucus. Biophys J. 2001; 81(4):1930–1937. [PubMed: 11566767]
14. Nance EA, et al. A dense poly(ethylene glycol) coating improves penetration of large polymeric nanoparticles within brain tissue. Sci Transl Med. 2012; 4(149):149ra119.
15. Wang YY, et al. Addressing the PEG mucoadhesivity paradox to engineer nanoparticles that “slip” through the human mucus barrier. Angew Chem Int Ed Engl. 2008; 47(50):9726–9729. [PubMed: 18979480]
16. Suh J, Dawson M, Hanes J. Real-time multiple-particle tracking: applications to drug and gene delivery. Adv Drug Deliv Rev. 2005; 57(1):63–78. [PubMed: 15518921]
17. Kim AJ, et al. Use of Single-Site-Functionalized PEG Dendrons To Prepare Gene Vectors that Penetrate Human Mucus Barriers. Angewandte Chemie International Edition. 2013:n/a–n/a.
18. Odeblad E. The functional structure of human cervical mucus. Acta Obstet Gynecol Scand. 1968; 47:57–79. [PubMed: 5690885]

19. Parr EL, Parr MB. Immune responses and protection against vaginal infection after nasal or vaginal immunization with attenuated herpes simplex virus type-2. Immunology. 1999; 98(4):639–645. [PubMed: 10594699]
20. Elstein M. Functions and physical properties of mucus in the female genital tract. Br Med Bull. 1978; 34(1):83–88. [PubMed: 342055]
21. Sanders N, Rudolph C, Braeckmans K, De Smedt SC, Demeester J. Extracellular barriers in respiratory gene therapy. Adv Drug Deliv Rev. 2009; 61(2):115–127. [PubMed: 19146894]
22. Ensign LM, Cone R, Hanes J. Oral drug delivery with polymeric nanoparticles: The gastrointestinal mucus barriers. Adv Drug Deliv Rev. 2012; 64(6):557–570. [PubMed: 22212900]
23. Lichtenberger LM. The hydrophobic barrier properties of gastrointestinal mucus. Annu Rev Physiol. 1995; 57:565–583. [PubMed: 7778878]
24. Macierzanka A, et al. Adsorption of bile salts to particles allows penetration of intestinal mucus. Soft Matter. 2011; 7(18):8077–8084.
25. Lieleg O, Vladescu I, Ribbeck K. Characterization of particle translocation through mucin hydrogels. Biophys J. 2010; 98(9):1782–1789. [PubMed: 20441741]
26. Allen E. The oestrous cycle in the mouse. American Journal of Anatomy. 1922; 30(3):297–371.
27. Dalal SJ, Estep JS, Valentin-Bon IE, Jerse AE. Standardization of the Whitten Effect to induce susceptibility to Neisseria gonorrhoeae in female mice. Contemp Top Lab Anim Sci. 2001; 40(2): 13–17. [PubMed: 11300681]
28. Zeitlin L, Whaley KJ, Hegarty TA, Moench TR, Cone RA. Tests of vaginal microbicides in the mouse genital herpes model. Contraception. 1997; 56(5):329–335. [PubMed: 9437563]
29. Asscher AW, Turner CJ, Deboer CH. Cornification of the Human Vaginal Epithelium. J Anat. 1956; 90(4):547. [PubMed: 13366869]
30. Smith BG, Brunner EK. The structure of the human vaginal mucosa in relation to the menstrual cycle and to pregnancy. American Journal of Anatomy. 1934; 54(1):27–85.
31. Moench TR, Mumper RJ, Hoen TE, Sun M, Cone RA. Microbicide excipients can greatly increase susceptibility to genital herpes transmission in the mouse. BMC Infect Dis. 2010; 10(331)
32. Wilson SS, et al. Susceptibility to genital herpes as a biomarker predictive of increased HIV risk: expansion of a murine model of microbicide safety. Antivir Ther. 2009; 14(8):1113–1124. [PubMed: 20032541]
33. Woodrow KA, et al. Intravaginal gene silencing using biodegradable polymer nanoparticles densely loaded with small-interfering RNA. Nat Mater. 2009; 8(6):526–533. [PubMed: 19404239]
34. Cu Y, Booth CJ, Saltzman WM. In vivo distribution of surface-modified PLGA nanoparticles following intravaginal delivery. J Control Release. 2011; 156(2):258–264. [PubMed: 21763739]
35. Kanazawa T, et al. Effective vaginal DNA delivery with high transfection efficiency is a good system for induction of higher local vaginal immune responses. J Pharm Pharmacol. 2009; 61(11): 1457–1463. [PubMed: 19903370]
36. Seavey MM, Mosmann TR. Estradiol-induced vaginal mucus inhibits antigen penetration and CD8(+) T cell priming in response to intravaginal immunization. Vaccine. 2009; 27(17):2342–2349. [PubMed: 19428849]
37. Kirch J, et al. Optical tweezers reveal relationship between microstructure and nanoparticle penetration of pulmonary mucus. Proc Natl Acad Sci U S A. 2012; 109(45):18355–18360. [PubMed: 23091027]
38. Suk JS, et al. The penetration of fresh undiluted sputum expectorated by cystic fibrosis patients by non-adhesive polymer nanoparticles. Biomaterials. 2009; 30(13):2591–2597. [PubMed: 19176245]
39. Schuster BS, Suk JS, Woodworth GF, Hanes J. Nanoparticle diffusion in respiratory mucus from humans without lung disease. Biomaterials. 2013
40. Lai SK, et al. Drug carrier nanoparticles that penetrate human chronic rhinosinusitis mucus. Biomaterials. 2011; 32(26):6285–6290. [PubMed: 21665271]
41. Louissaint NA, et al. Distribution of cell-free and cell-associated HIV surrogates in the female genital tract after simulated vaginal intercourse. J Infect Dis. 2012; 205(5):725–732. [PubMed: 22279121]

42. Louissaint NA, et al. Distribution of Cell-free and Cell-associated HIV surrogates in the Colon Following Simulated Receptive Anal Intercourse in Men who Have Sex with Men. J Acquir Immune Defic Syndr. 2012

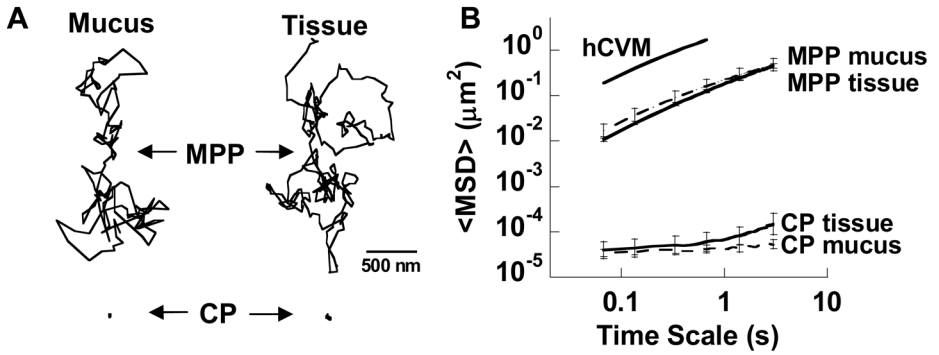

Figure 1.

Comparison of MPP and CP transport in colon mucus and on *ex vivo* colon tissue. (A) Representative trajectories for 100 nm MPP and CP particles exhibiting diffusivities within one SEM of the ensemble average at a time scale of 1 s in collected colon mucus (Mucus) or on *ex vivo* colon tissue (Tissue). (B) Ensemble-averaged geometric mean square displacements (<MSD>) of MPP and CP as a function of time scale in mucus or on tissue. Data compared to the same particles in collected human CVM (hCVM) (2). Data represent the ensemble average of three independent experiments using mucus or tissue from three different mice, with n ≥ 140 particles for each experiment and an average of n = 151 and 156 for MPP and CP, respectively.

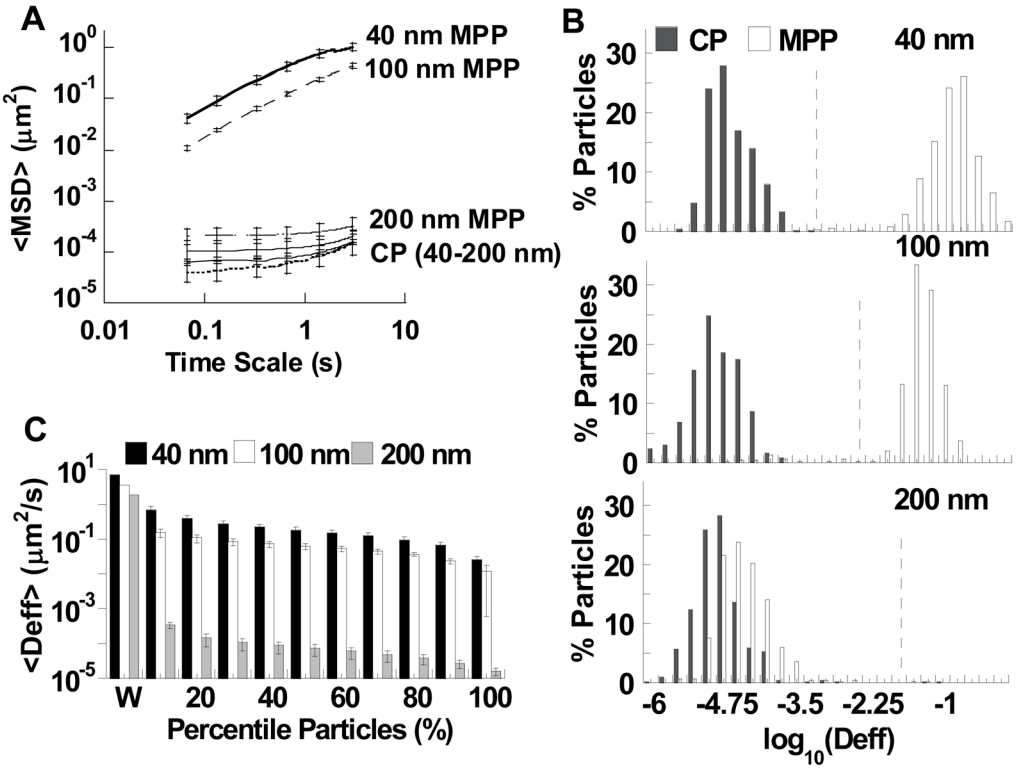

Figure 2.

Transport of MPP and CP on *ex vivo* colon tissue. (A) Ensemble-averaged geometric mean square displacements (<MSD>) of MPP and CP as a function of time scale on *ex vivo* colon tissue. (B) Distributions of the logarithms of individual particle effective diffusion coefficients (Deff) at a time scale of 1 s for for 40, 100, and 200 nm MPP. Diffusivity values to the left of the dotted line indicate particles with MSD values less than the particle diameter, indicating that particle motion is due to thermal fluctuation of the mucus gel and not diffusion. (C) Comparison of average D_{eff} ($<D_{eff}>$) of subfractions of particles, from fastest to slowest, at a time scale of 1 s to the theoretical diffusion coefficient in water (W) Data represent the ensemble average of three independent experiments using tissue from three different mice, with n ≥ 121 particles for each experiment and an average of n = 151 and 152 for MPP and CP, respectively.

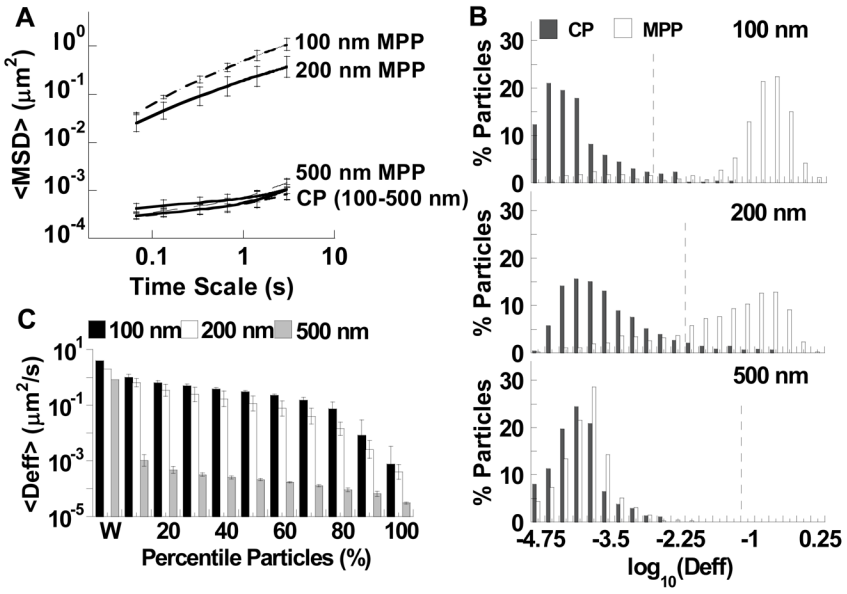

Figure 3.

Transport of MPP and CP on *ex vivo* small intestine tissue. (A) Ensemble-averaged geometric mean square displacements (<MSD>) of MPP and CP as a function of time scale on *ex vivo* small intestine tissue. (B) Distributions of the logarithms of individual particle effective diffusion coefficients (D_{eff}) at a time scale of 1 s for for 100, 200, and 500 nm MPP. Diffusivity values to the left of the dotted line indicate particles with MSD values less than the particle diameter, indicating that particle motion is due to thermal fluctuation of the mucus gel and not diffusion. (C) Comparison of average D_{eff} ($<D_{eff}>$) of subfractions of particles, from fastest to slowest, at a time scale of 1 s to the theoretical diffusion coefficient in water (W). Data represent the ensemble average of three independent experiments using tissue from three different mice, with $n \geq 136$ particles for each experiment and an average of n = 165 and 159 for MPP and CP, respectively.

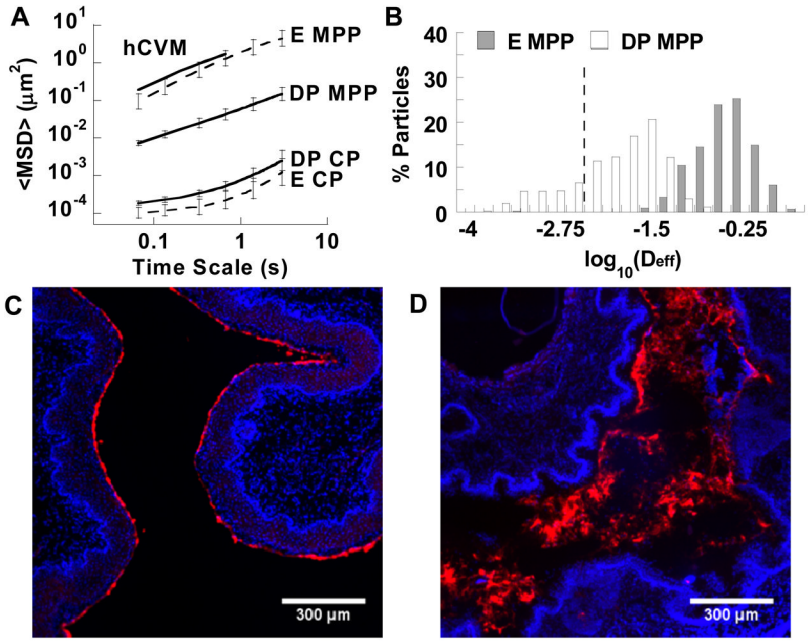

Figure 4.

Transport rates of 100 nm CP and MPP on *ex vivo* tissue from mice in the estrus phase (E) (1) or from mice treated with DP (DP). (A) Ensemble-averaged geometric mean square displacements (<MSD>) as a function of time scale. Data for particles on *ex vivo* mouse vaginal tissue compared to the same particles in human *ex vivo* CVM (hCVM) (2). (B) Distributions of the logarithms of individual MPP particle effective diffusion coefficients (D_{eff}) at a time scale of 1 s. Diffusivity values to the left of the dotted line indicate particles with MSD values less than the particle diameter, indicating that particle motion is due to thermal fluctuation of the mucus gel and not diffusion. Distribution of 100 nm MPP in the vagina of (C) estrus phase and (D) DP mice, 10 min after administration. Data represent the ensemble average of three independent experiments using tissue from three different mice, with n ≥ 120 particles for each experiment and an average of n = 155 and 150 for MPP and CP, respectively.

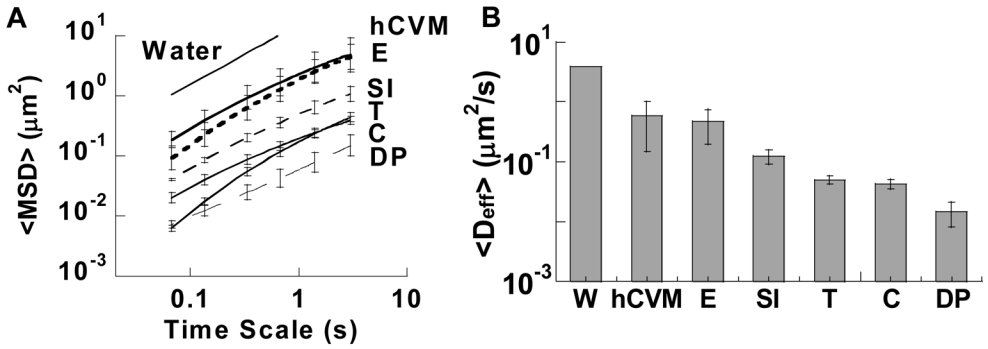

Figure 5.

Comparison of the transport rates of 100 nm MPP on mouse *ex vivo* tissues. (A) Ensemble-averaged geometric mean square displacements (<MSD>) as a function of time scale. Data for particles on *ex vivo* mouse estrus phase vaginal (E) (1), small intestine (SI), trachea (T), colon (C), and DP vaginal tissue compared to theoretical diffusion of 100 nm particles in pure water (Water) and diffusion of 100 nm particles in hCVM (hCVM) (2). (B) Ensemble-averaged effective diffusion coefficients (<D_{eff}>) at a time scale of 1 s compared to the theoretical diffusion coefficient in pure water (W) and in hCVM (2).

Table 1

Particle characterization

Size (nm)*	CP/MPP	Diameter (nm)	ζ-potential (mV)
40	CP	56 ± 2	−33 ± 0.6
100	CP	87 ± 4	−39 ± 2.4
200	CP	190 ± 3	−53 ± 1.5
500	CP	500 ± 11	−69 ± 2.7
40	MPP	60 ± 1	−2.2 ± 0.2
100	MPP	108 ± 1	−3.3 ± 0.5
200	MPP	212 ± 4	−4.0 ± 0.3
500	MPP	524 ± 5	−3.9 ± 0.1

* as provided by manufacturer